ISSN 1727-7337 (print)
ISSN 2663-2217 (online)

UDC 621.454.2.034-046.62.01 **doi: 10.32620/aktt.2022.4sup1.13**

Maurício Sá GONTIJO

Instituto Tecnológico de Aeronáutica, Aeronautic Engineering and Mechanics, Aerospace Propulsion and Energy, Brazil

A REVIEW OF VAPORIZATION MODELS AS DESIGN CRITERION FOR BIPROPELLANT THRUST CHAMBERS

In the beginning of liquid propellant rocket engine development, the thrust chamber sizes were obtained, mainly, empirically. With the technological advancements over the years, several approaches have been developed in order to optimize its sizes and predict more accurately the performance. Besides the clear contribution in predicting efficiencies, the use of accurate vaporization models to optimize combustion chambers decreases losses and the number of required tests. To increase efficiencies, the chamber must be optimized. In case the chamber is too small, incomplete combustion is achieved and combustion instability may occur. In case the chamber is too large, losses due to weight and heat transfer increase and the vehicle becomes larger (leading to more drag losses). Additionally, the number of tests is reduced since models were experimentally validated and less experimental iterations are required in order to obtain the optimized design. Although there are many models, all of them reach similar conclusions, such as an increase in chamber pressure, a decrease in injected droplet size and velocity, and others, lead to a decrease in the required chamber size. Nowadays, with the advancements in computing budget, more complex and accurate models have be developed. Some of these models account for chemical reactions, turbulence effects, droplet collisions and interactions, two- and three-dimensional modeling, and others. Also, the use of CFD codes provides relevant contributions to the analytical and numerical models, especially in validating them, and, additionally, decreases the amount of required experimental tests. The main propulsive parameter that rules this phenomenon is the characteristic length, which accounts the required chamber size for the propellants to be injected, atomized, vaporized, mixed and combusted. Most of the available models neglect the atomization, mixing and combustion of the propellant, since those phenomena occur much faster compared with the vaporization. This work provides a review of those vaporization models, focusing on the main used models worldwide. Such review is of great importance in order to supply enough information and comparison between models, making possible for the researcher/engineer to choose the model that better fit its necessities, requirements and limitations.

Keywords: *vaporization models; liquid propellant rocket engines; characteristic length; injected droplet size.*

Introduction

Droplet vaporization models have been widely used to design the injectors and combustion chambers of Liquid Propellant Rocket Engines (LPRE). All of these models are related with the characteristic length (L^*), which defines the required space for complete propellant injection, atomization, vaporization, mixing and combustion. The L^* is mathematically defined below:

$$L^* = \frac{V_c}{A_t} = \frac{\dot{m} V t_s}{A_t}, \qquad (1)$$

where V_c is the chamber volume, A_t is the throat area, V is the average specific volume in the chamber, and t_s is the residence time or stay time. Many references present tabulated data of L^*, such as [1, 2]. However, using tabulated data isn't the ideal, since it is presented only in function of the propellant mixture.

From the phenomena taking place inside the combustion chamber, the one that takes more time to finish is the vaporization itself. The injection is simply the act of injecting the propellants through the injectors. The atomization in rocket engines, in general, happens almost instantaneously after the injection, due to the commonly obtained Reynolds, Weber and Ohnesorge numbers [3-6]. Mixing is also achieved very fast, since droplets are oftenly colliding. And, combustion and chemical reactions are commonly neglected in vaporization models assuming it occurs in an infinitesimal time step [7-12]. With these statements, it is quite accurate to calculate the chamber size with vaporization models.

Definitely the vaporization rate is highly impacted by the thermophysical properties of droplet, however there are many of other parameters that are even more relevant. The injector design is one of the main factors that impacts on how fast the droplet will vaporize, since it defines directly the injected droplet size and velocity. The faster and the larger is the droplet, the longer the chamber must be. In addition, the properties of the combustion products gas and the chamber design plays an important role in such type of analysis, as it will be discussed in this work.

One of the most used approaches to calculate, theoretically, the droplet size is through the SMD (Sauter Mean Diameter), also known as D_{32} or the MMD (Mass Mean Diameter), also known as $D_{0.5}$. These are, in general, empirically derived statistical equations in a wide range of experiments. The recommended is to obtain these equations for each propellant, since most of the presented equations in literature were obtained for other fluids [5]. There are other ways of calculating the droplet size, but SMD and MMD are the most used.

The injection velocity is easily obtained, for incompressible fluids, through the following equation:

$$v_i = \sqrt{\frac{2\Delta P}{\rho}}, \qquad (2)$$

where ΔP is the pressure drop across the injector and ρ is the propellant density. The pressure drop can be defined as 30% of the chamber pressure, if throttling, or 20%, if not throttling [2]. [1] recommends 20%. Other approach is using the following relation from [13] in function of the chamber pressure P_c (in Pa for these relations):

$$\Delta P = \begin{cases} 80\sqrt{10P_c}; & \text{if liquid propellant} \\ 20\sqrt{10P_c}; & \text{if gaseous propellant} \end{cases}, \qquad (3)$$

The Fig. 1 shows how the injection velocity and the pressure drop varies with chamber pressure for liquid propellants assuming $\rho = 1400\ \text{kg/m}^3$.

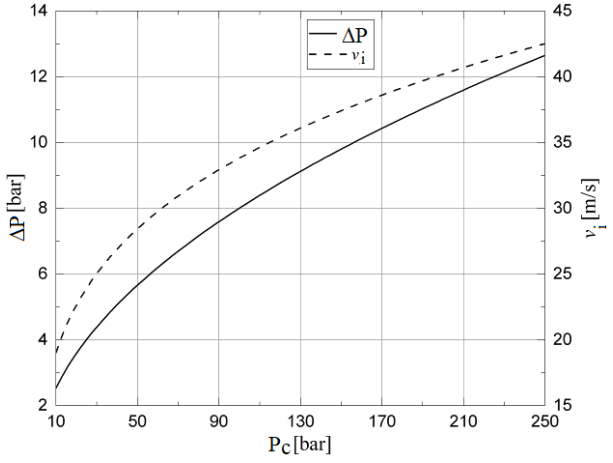

Fig. 1. Variation of ΔP and v_i with P_c with constant ρ

Also, the nozzle contraction ratio plays a relevant role since it impacts directly on the final gas velocity inside the combustion chamber. The final gas velocity is calculated through the Area-Mach relation with Mach = 1 in the throat [14-16], shown below:

$$\frac{A_c}{A_t} = \frac{1}{M_c}\sqrt{\left[\frac{2}{\gamma_c+1}\left(1+\frac{\gamma_c-1}{2}M_c^2\right)\right]^{\frac{\gamma_c+1}{\gamma_c-1}}}, \qquad (4)$$

where A_c and A_t are the chamber and throat areas, respectively, and M_c and γ_c are the Mach number and the specific heat ratio at the nozzle inlet, respectively. The M_c is obtained through equation (4) and the velocity at the nozzle inlet is calculated below:

$$v_c = M_c a_c = M_c\sqrt{\gamma_c R T_c}, \qquad (5)$$

where a_c is the sound speed at the end of the combustion chamber/nozzle inlet, T_c is the adiabatic flame temperature inside chamber and R is the gas constant.

The faster is the gas at the nozzle inlet, the larger is the chamber. By analyzing the equation (4), it is possible to determine that the lower is the contraction ratio, the higher is v_c. Then, in terms of L^*, the contraction ratio must be the highest possible. However, high contraction ratios are not commonly used since it may lead to boundary layer instabilities upstream the throat, higher heat transfer, manufacturing complications, diameter limitations and others. In general, the contraction ratio lays between 1.5 and 3 [17, 18].

The chamber size must be optimized in order to achieve the highest performance, since the L^* affects directly the characteristic velocity C^* [1,7,10-12,17,19]. This is due to the fact that if the chamber is too short, incomplete combustion is achieved inside the combustion chamber and may lead to combustion instabilities [20]. In the other hand, if the chamber is too large, losses due to heat transfer and increase in weight and costs become impeditive [1,19]. The relation between t_s, L^* and C^* is the following:

$$C^* = \frac{t_s P_c}{\rho_c L^*}. \qquad (6)$$

Therefore, this type of analysis is of substantial relevance in designing a LPRE thrust chamber.

Early developments

One of the first models was published by Priem [7, 21-24]. In those works, it was presented a system of equations describing the vaporization model. This system of equations was developed by the statement that the vaporization on a droplet is mainly ruled by mass and energy conservation laws and by the interaction between the liquid of the droplet with the vapor film and the vapor film with the gas atmosphere [7,10-12,21-25]. In addition, the following assumptions were made:

1) One-dimensional model
2) No combustion and chemical reactions;
3) No breakup process;

ISSN 1727-7337 (print)
ISSN 2663-2217 (online)

4) Spherical droplets;
5) Constant thermophysical properties of the gas;
6) One-dimensional model;
7) No droplets interactions;
8) Only convective heat transfer;
9) All droplets are injected with same size, velocity and temperature;
10) Transient model under steady state engine operation.

According to the above assumptions, the equations of mass transfer, heat transfer, droplet heating rate, droplet acceleration and gas velocity could be derived as shown below, respectively:

$$\frac{dm}{dt} = A_d K \varsigma P_d; \tag{7}$$

$$q = hA_d\left(T_c - T_d\right)Z; \tag{8}$$

$$\frac{dT_d}{dt} = \frac{q - \frac{dm}{dt}\lambda}{mc_{p,L}}; \tag{9}$$

$$\frac{dv_d}{dt} = \frac{3Sv_{rel}{}^2\rho vg}{8r_{d\rho L}}; \tag{10}$$

$$v_g\left(x\right) = a_c M_c\left(1 - \frac{\dot{m}_f\left(x\right)}{\dot{m}_f\left(m=0\right)}\right), \tag{11}$$

where m is the droplet mass, A_d, P_d, T_d and r_d are the droplet surface area, partial pressure, temperature and radius, respectively, K is the mass transfer coefficient, ζ is the correction factor for unidirectional mass transfer, h is the heat transfer coefficient, T_c is the adiabatic flame temperature inside chamber, Z is a term for the account of the sensible heat taken up by the diffusing vapor, λ is the droplet latent heat of vaporization at temperature T_d, $c_{p,L}$ and ρ_L are the droplet in liquid phase specific heat at constant pressure and density, respectively, v_d is the droplet velocity, v_{rel} is the relative velocity, ρ_{vg} is the vapor-gas mixture density, v_g is the gas velocity and $\dot{m}_f$ is the mass flow rate of vaporization of the fuel. Is valid to remember that when the droplet vaporizes there is: $v_g(x=L_c) = v_g(m=0) = v_c$. The image below represents better how each of the equations (7) - (11) acts on the droplet inside the chamber control volume (CV).

The mass transfer coefficient is calculated through:

$$K = \frac{ShM_v D}{2r_d R_u \bar{T}} = \frac{\left(2 + 0.6\sqrt[3]{Sc}\sqrt{Re}\right)M_v D}{d_d R_u \bar{T}}, \tag{12}$$

where Sh is the Shearwood number, obtained through Ranz Marshall relation [26], M_v is the molecular weight of vaporizing species, D is the mass diffusivity, r_d is the droplet radius, R_u is the universal gas constant and $\bar{T}$ is the average temperature $\left(\bar{T} = \left(T_c + T_d\right)/2\right)$, d_d is the droplet diameter, Sc is the Schmidt number and Re is the Reynolds number, both are calculated below:

$$Re = \frac{\rho vc}{\mu}, \tag{13}$$

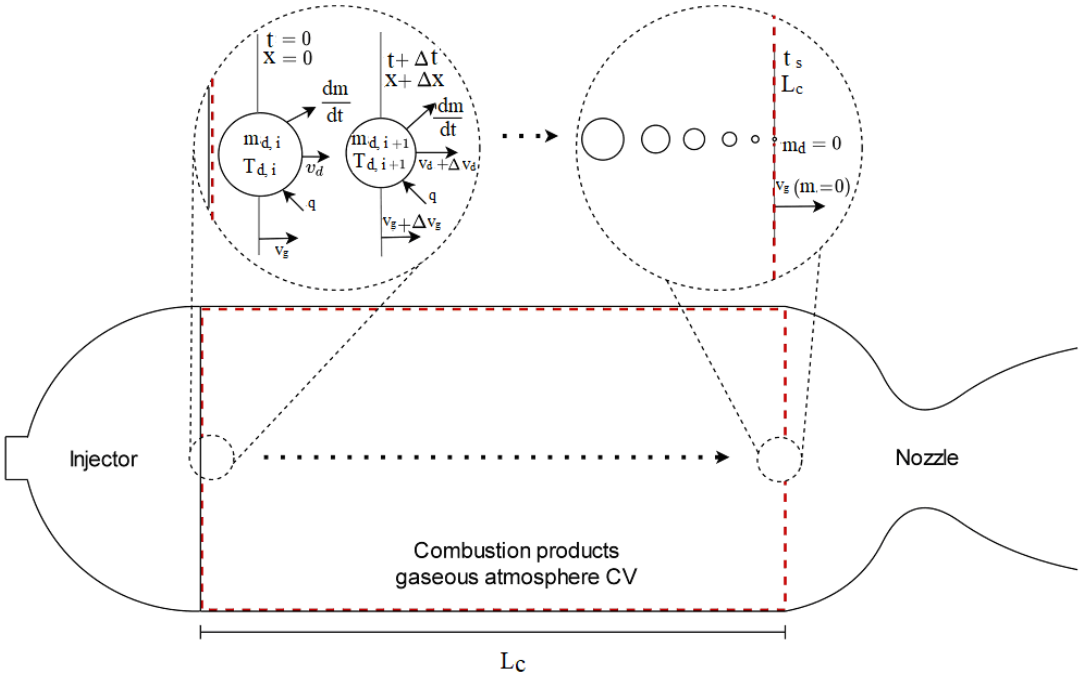

Fig. 2. Scheme of Priem's model of governing equations acting on the droplet inside a gaseous atmosphere

$$Sc = \frac{\mu}{\rho D}, \tag{14}$$

where c is the characteristic dimension, v is the velocity and μ is the dynamic viscosity. The correction factor ζ is obtained through:

$$\varsigma = \frac{P_c}{P_d} \ln\left(\frac{P_c}{P_c - P_d}\right). \tag{15}$$

The parameter Z is defined below:

$$Z = \frac{z}{\left(e^z - 1\right)}, \tag{16}$$

where z is calculated by:

$$z = \frac{\frac{dm}{dt} c_p t_f}{4 k_m r_d \left(r_d + t_f\right)}, \tag{17}$$

where t_f is the gas film thickness and k_m is the mean value of thermal conductivity, defined as:

$$k_m = \left(1 - \frac{P_d/P_c}{2}\right) k_d + \frac{P_d/P_c}{2} k_g, \tag{18}$$

where k_d and k_g are the thermal conductivity of the droplet and the gas, respectively. The heat transfer coefficient h is calculated through:

$$h = \frac{k_m Nu}{d_{\bar{d}|}} = \frac{k_m \left(2 + 0.6 \sqrt[3]{Pr} \sqrt{Re}\right)}{d_{\bar{d}|}}, \tag{19}$$

where Nu is the Nusselt number, obtained through Ranz Marshall relation [26], and Pr is the Prandtl number, which is calculated below:

$$Pr = \frac{c_p \mu}{k}, \tag{20}$$

where k is the thermal conductivity.

The drag coefficient from the drag law for a spherical object [27] is defined as:

$$S = 27\, Re^{-0.84}. \tag{21}$$

The equation above was derived for a range of Re from 6 to 400, but [24] successfully tested it for propellant droplets for ranges up to 2000. Other relations for S exist and some are presented by [28,29]. Finally, the vapor-gas mixture density is obtained through:

$$\rho_{vg} = \frac{P_c \bar{M}}{R_u \bar{\bar{T}}}, \tag{22}$$

where $\bar{M}$ is the average molecular weight between vaporizing droplet and gas and is calculated through:

$$\bar{M} = \left(1 - \frac{P_d/P_c}{2}\right) M_d + \frac{P_d/P_c}{2} M_g, \tag{23}$$

where M_d and M_g are the molecular weight of the droplet and gas, respectively. In [4] also discussed this one-dimensional vaporization-controlled combustion model and [30] presented a similar model to Priem's model. In [7,23] it is also presented the effective length, which is a correction factor to be added on Priem's model.

At the same decade as Priem, Spalding also developed an interesting model. In Spalding's model, it was used a dimensionless approach where a system of equations was solved in order to obtain a simple analytical equation to calculate the L^*. The same assumptions valid for Priem's model is valid for Spalding's with the addition that a binary diffusion with Lewis number equal to 1 is assumed [8,31,32]. The dimensionless system of equations is composed by the change in droplet radius, droplet velocity, distance traveled, vaporization rate, drag law, gas velocity and chemical load, which is shown below, respectively:

$$\zeta_r = r_d / r_0; \tag{24}$$

$$\chi_r = \rho_g v / G; \tag{25}$$

$$\xi_r = R_0 \rho_g x / G r_0; \tag{26}$$

$$\beta_r = R_r / R_{r,0}; \tag{27}$$

$$S_r = 9\mu_g / 2 R_0 r_0 \rho_L; \tag{28}$$

$$\omega_r \equiv \rho_g \mu / \dot{m}; \tag{29}$$

$$L_r \equiv R_0 [c_{p,g}(T_c - T_v) + q_r] \rho_g / \dot{q}'''_m r_0, \tag{30}$$

where r_0 is the initial droplet radius, R_r is defined at equation (32) and $R_{r,0}=R_r$ with droplet in entry state and gas in equilibrium, $\dot{m}$ is the propellant mass flow rate, the subscript 0 relates to initial, L to liquid and g to gas, $\dot{q}'''_m$ is the maximum value of the volumetric energy release rate and G is the propellant mass flux calculated below. Since no combustion and no chemical reactions is assumed, the chemical load L_r is taken to be 0.

$$G = \frac{\dot{m}}{A_c}; \tag{31}$$

$$R = \frac{\left(k / c_{p,g} \rho_L\right) \ln\left(1 + B\right)}{r_d}, \tag{32}$$

where B is the Spalding number or transfer number, defined as (for Le=1, which means: $B_T = B_M$, where B_T is the thermal energy transfer number equal to the equation defined below and B_M is the mass transfer number $B_M = Y_{fs} / \left(1 - Y_{fs}\right)$, where Y_{fs} is the fuel mass fraction at the droplet surface[32-34]):

ISSN 1727-7337 (print)
ISSN 2663-2217 (online)

$$B = c_{p,g}\frac{T_c - T_s}{Q_b}, \tag{33}$$

where T_s is the surface temperature of the droplet ($T_s = T_d$) and Q_b is the heat of vaporization. Fig.3 shows a representation of the governing dimensionless equations.

Solving the governing equations and with their respective, not presented here but well derived at [8,35], the following relations are obtained:

$$\omega_r = 1 - \zeta_r^3; \tag{34}$$

$$\chi_r = \left(\frac{\chi_0 + 3}{S_r - 3}\right)\zeta_r^{S_r} + 1 - \left(\frac{\zeta_r^3 S_r}{S_r - 3}\right); \tag{35}$$

$$\xi_r = \frac{\frac{\chi_0 + 3}{S_r - 3}\left(1 - \zeta_r^{Sr+2}\right)}{S_r + 2} + \frac{1 - \zeta_r^2}{2} - \frac{S_r\left(1 - \zeta_r^{S_r}\right)}{5(\beta - 3)}. \tag{36}$$

Here, now, by solving equations (28) and (32), the S_r is taken to be:

$$S_r = \frac{9\,Pr}{2\ln(1+B)} \cong \frac{9\,Pr}{2B} \tag{37}$$

where χ_0 is the ratio of the injected velocity by the final gas velocity, $\chi_0 = v_i / v_c$. Some graphical solutions of the above equations are shown in Fig. 4, for a fixed value of S_r=0.5 and three values of χ_0 equal to 0.2, 0.5 and 1, respectively.

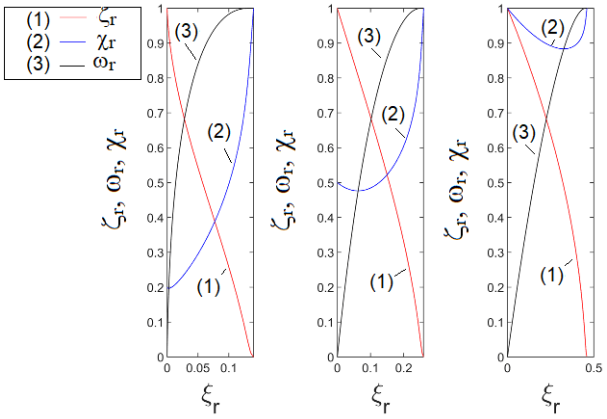

Fig. 4. Variation of ζ_r, ω_r and χ_r for S_r=0.5 and χ_0 equal to 0.2, 0.5 and 1, respectively

For the case where the boundary conditions achieved at the nozzle inlet (Fig. 3) is applied, the minimum dimensionless length is reached and calculated through:

$$\xi^* = \frac{\chi_0 + 0.3S_r}{2 + S_r} = \frac{v_i / v_c + 0.3S_r}{2 + S_r}. \tag{38}$$

Finally, the characteristic length equation is presented below:

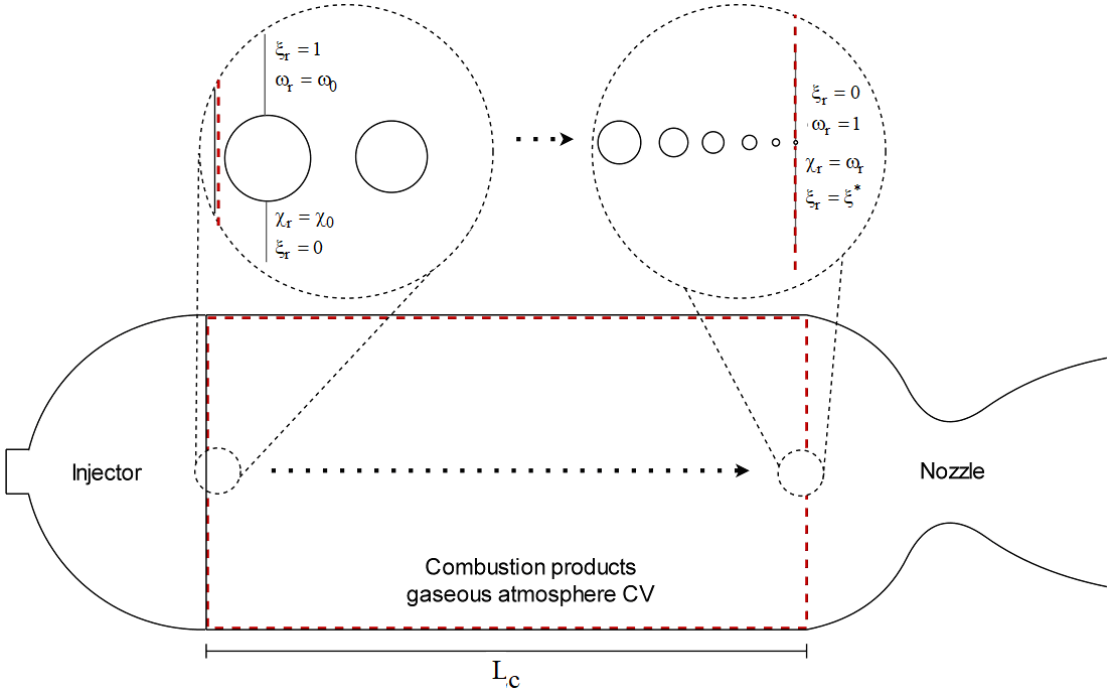

Fig. 3. Scheme of Spalding's model of governing equations acting on the droplet inside a gaseous atmosphere

$$L^* = \xi^* r_0^2 \left[\frac{2}{\gamma_c + 1} + \left(\frac{G}{\rho_c \sqrt{\gamma_c R T_c}} \right)^2 \frac{\gamma_c - 1}{\gamma_c + 1} \right]^{\frac{\gamma_c + 1}{2(\gamma_c - 1)}} \frac{c_{p,c} \rho_L}{k} \frac{\sqrt{\gamma_c R T_c}}{\ln(1+B)}. \quad (39)$$

The Fig. 5 shows how ξ^* varies with S_r for some values of χ_0.

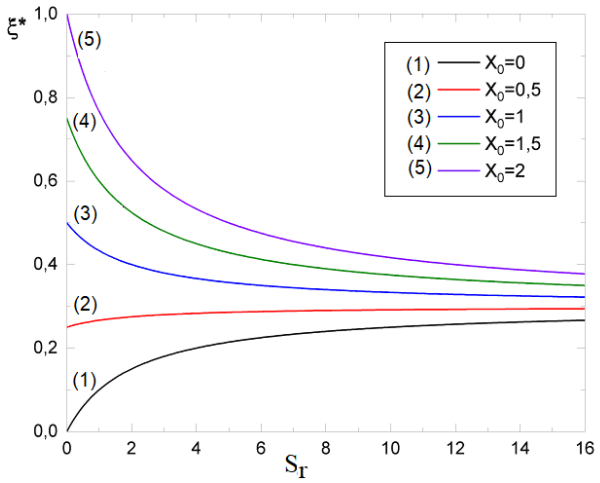

Fig. 5. Variation of ξ^* with S_r for some values of χ_0

This theory was also used in gas generators [36]. An analysis made at [9] shows that the injector design has more than 58 % of impact in the L^* for a specific engine, which is another way to prove that using tabulated data is not even close to ideal. A contribution to the Spalding's model made by [9,37,38] was the introduction of the characteristic equivalence ratio, ϕ^*, which is defined as the equivalence ratio required to reach the minimum characteristic length for a given chamber pressure. The φ^* is mathematically defined as:

$$\phi^* = \left(\frac{F/O}{(F/O)_{st}} \right)_{\downarrow L^*} = \left(\frac{\dot{m}_f / \dot{m}_o}{(\dot{m}_f / \dot{m}_o)_{st}} \right)_{\downarrow L^*}. \quad (40)$$

Also, some studies were made in order to include convective effects on [8,9]. Also, Adler [39] made some contributions by adding the chemical reaction rate influence. To account for this addition, a relation is defined for the fractional decrease in the droplet radius below:

$$\eta = \frac{r_0 - r_d}{r_d} = 1 - \zeta_r = 1 - \frac{r_d}{r_0}. \quad (41)$$

In addition, dimensionless differential equations of the droplet velocity must be used and is calculated by the following equation:

$$\frac{d\chi_r}{d\eta} = \frac{S_r}{(1-\eta)\tau} \left[\iota\left(\eta^2 - 3\eta + 3\right) - \chi_r \right], \quad (42)$$

where τ is the dimensionless temperature or reacted ness and the dimensionless differential equation of τ is:

$$\frac{d\tau}{d\eta} = \frac{(1-\eta)}{\eta\left(\eta^2 - 3\eta + 3\right)} \left[\frac{\psi}{L_r \tau} \chi_r - 3(1-\eta)\tau \right], \quad (43)$$

where ψ is the dimensionless reaction rate function, which is defined by:

$$\psi(\tau) = (n+1)\left(1 + \frac{1}{n}\right)^n (1-\tau)\tau^n, \quad (44)$$

where *n* is an integer that modifies the form of the reaction rate. Now, the chemical loading is taken to be:

$$L_r = \frac{\chi_0 \cdot \psi(\tau_0)}{3\tau_0^2}. \quad (45)$$

The equation above was derived assuming that $\frac{d\tau}{d(1-\eta)} = 0$, since for the majority size of the droplet this is a reasonable approximation [39]. The value of L lays between 0 and a critical value L_c, which is obtained by combining equations (44) and (45) and is calculated through:

$$L_c = \frac{\chi_0}{3} \left(\frac{n+1}{n-1} \right) \left(1 + \frac{1}{n} \right)^n \left(1 + \frac{1}{n-1} \right)^{n-2}. \quad (46)$$

The L_c/χ_0 ratio informs that whether combustion is possible or not. If $L/\chi_0 < L_c/\chi_0$ the combustion is possible and chemical reactions must be considered. Finally, ξ^* is now calculated with the following equation:

$$\xi^* = \int_0^1 \frac{\chi_r}{\tau} \zeta_r d\zeta_r. \quad (47)$$

The boundary conditions to solve equation (47) are $\zeta_r = 0$, $\chi_r = 0$, v = v_g and $\tau = \tau_1 \le 1$. To solve equations (42) and (43), a fourth order Runge-Kutta numerical method is used. However, the first step of the numerical solution needs to be calculated analytically with:

$$\chi_1 = \chi_0 + \left(\frac{d\chi}{d\eta} \right)_0 h; \quad (48)$$

ISSN 1727-7337 (print)
ISSN 2663-2217 (online)

$$\tau_1 = \tau_0 + \left(\frac{d\tau}{d\eta}\right)_0 h, \qquad (49)$$

where h is an integration step size and it is defined as $h = -\eta + 1$. Also, equation (49) can be rewritten as:

$$\tau_1 = \tau_0 + \left[\frac{(s-\tau_0)(1-\tau_0)}{(n-2)(1-\tau_0)-1}\right] h. \qquad (50)$$

The boundary conditions to solve equations (48) and (49) are $\eta = 0$, $\chi_r = \chi_r$, and $\tau = \tau_0$.

The Fig. 6 shows how ψ varies with τ for some values of n and Fig. 7 shows the regions of possible combustion and impossible combustion based on L_c/χ_0.

Finally, an example of a graph of φ^* was presented in [37] for three propellant mixtures. In addition, logarithmic fittings were made, this get to be a very helpful tool on preliminary designs of LPRE thrust chambers. The Fig. 8 shows this graph and the logarithmic fitting are shown in [37]. In addition, since now combustion is taking place, another form of the B may be used [32]. Thus, the transfer number becomes:

$$B = \frac{H}{Q_b}\frac{m_{o_2 g}}{r} + c_{p,g}\frac{T_c - T_s}{Q_b}, \qquad (51)$$

where H is the calorific value of fuel, $m_{o_2 g}$ is the weight concentration of oxygen and r is the weight of oxygen required for combustion of unit weight fuel. More interesting discussion of the Spalding's model is presented in [40]. Various typical transfer numbers are compiled in [41].

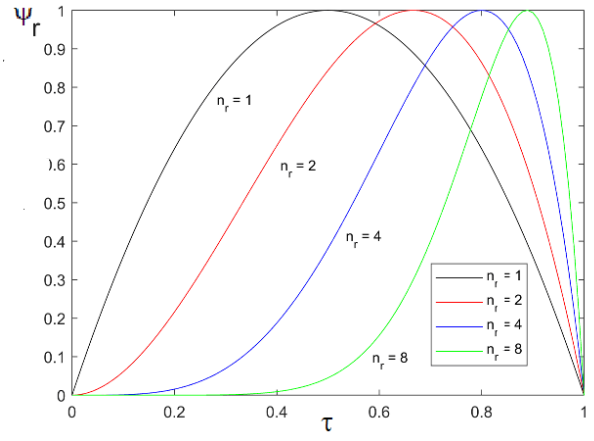

Fig. 6. Variation of ψ with τ for some values of n

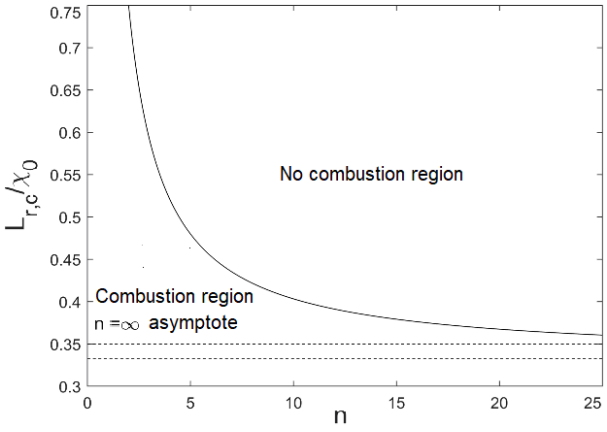

Fig. 7. Regions of possible combustion and impossible combustion based on L_c/χ_0

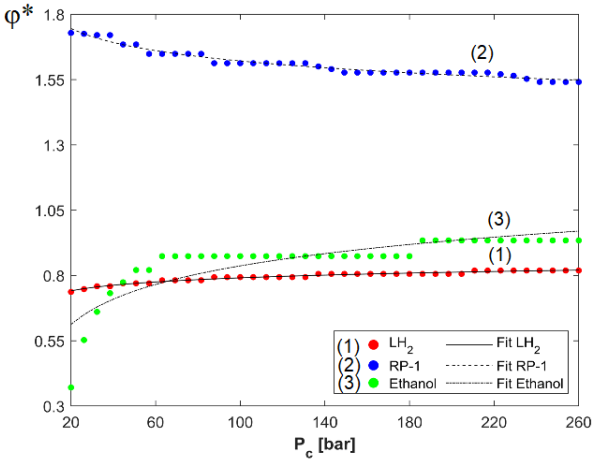

Fig. 8. Variation of φ* with chamber pressure

Considerations to combustion instability

As previously stated, the droplets vaporization is related to some types of combustion instabilities. The most related type is the feed system coupled instability, or the L* instability [20]. Starting from the continuity inside the thrust chamber, the ideal gas law and Bernoulli's equation, the following expression is obtained:

$$\frac{RT_c}{V_c} C_d A_i \sqrt{2\rho(P_i - P_c)} = \frac{RT_c}{V_c} C_d A_i \sqrt{2\rho(P_i - \bar{P}_c)}\left(1 - \frac{\dot{P}_c}{P_i - \bar{P}_c}\right)^{1/2}, \qquad (52)$$

where C_d is the discharge coefficient, A_i is the injection area, t is the time, t_c is the combustion delay time, $\bar{P}_c$ is the average chamber pressure and $\dot{P}_c$ is the pressure oscillation around $\bar{P}_c$, then $P_c = \bar{P}_c + \dot{P}_c$. By applying

Taylor series, by assuming that $\phi = \dot{P}_c / \bar{P}_c$ and that $\beta = \frac{\bar{P}_c}{2(P_i - P_c)}$, and remembering that t_s may be calculated by $t_s = \frac{L^*}{C^* \Gamma^2}$, where Γ is the Vandenkerckhove function [42], equation (52) turns to be:

$$\frac{dP_c}{dt} = \frac{\bar{P}_c}{t_s}\left[1 - \beta\phi\left(t - t_c\right)\right] - \frac{P_c}{t_s}. \qquad (53)$$

Taking the differential form of ϕ and substituting in equation (53) the following equation is achievable:

$$\frac{d\phi}{dt} + \frac{\phi}{t_s} = \left(\frac{\phi\beta}{t_s}\right)_{t-t_c}. \qquad (54)$$

The solution of the above equation is of the form $\phi = A\cos\omega t = \mathrm{Re}\left\{Ae^{(-i\omega t)}\right\}$ and $\phi = A\sin\omega t = \mathrm{Im}\left\{Ae^{i\omega t}\right\}$, where ω is the angular frequency ($\omega = 2\pi f$, where f is the frequency). With these solutions and equation (54), the real and imaginary solutions are:

$$\begin{cases} \alpha + \frac{1}{t_s} = -\frac{\beta}{t_s} e^{-\alpha t_s} \cos\omega t_s & ; \text{Real} \\ \omega = -\frac{\beta}{t_s} e^{-\alpha t_s} \sin\omega t_s & ; \text{Imaginary} \end{cases} \qquad (55)$$

where α represents the growth in oscillation amplitude. By the solutions above, when α = 0 the combustion is stable and there is no pressure oscillation. By combining the solutions above when α = 0 it is achieved the critical value, in which characterizes the stable and unstable regions. The Fig. 9 shows these two regions and the critical curve defined by α = 0 and the resulting expression that describes this curve, originated from equation (56). In addition, if α > 0 the combustion is stable and if α < 0 it is unstable. Fig. 9 shows a representation of each scenario.

Other possible discussion is, as seen in Fig. 9, when α = 0 and $t_c \to \infty$, then $\beta \to 1$. Under this condition, it is defined the Summerfield stability criterion showed below:

$$\frac{P_i - P_c}{\bar{P}_c} > 0.5 \to \frac{\Delta P}{\bar{P}_c} > 0.5. \qquad (56)$$

The relation above must be satisfied to guarantee stable combustion. However, it is possible to have a ΔP lower than 50% of the chamber pressure and still achieve stable combustion. This is explained by remembering that the Summerfield criterion is valid for α = 0 and $t_c \to \infty$ [20].

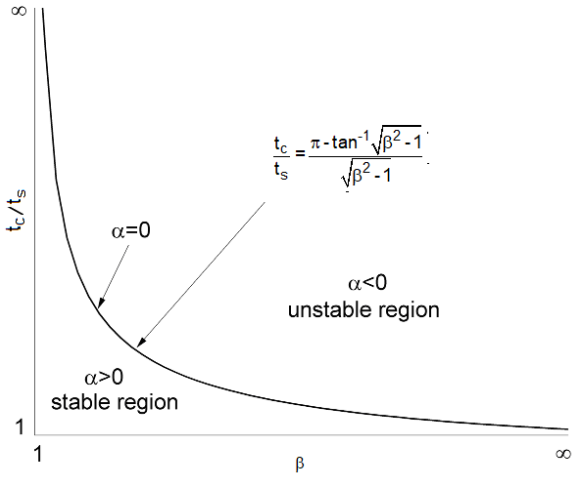

Fig. 9. Stability regions

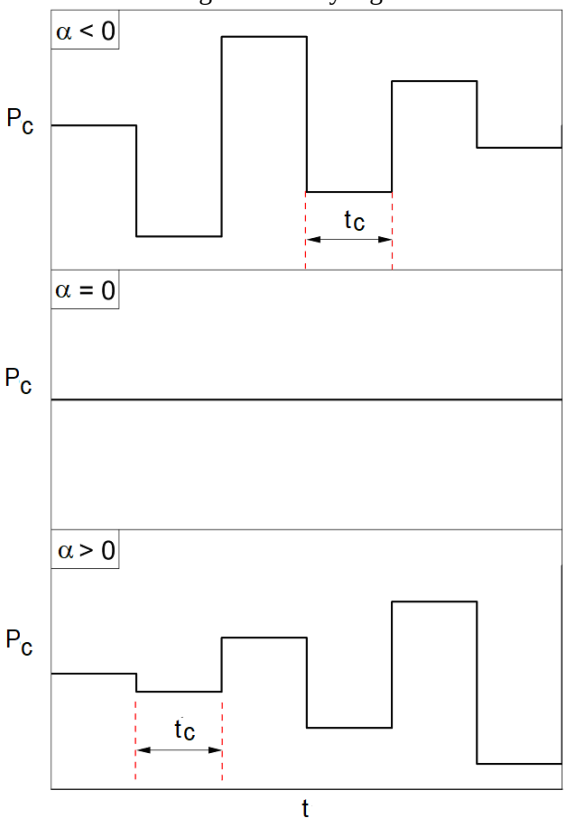

Fig. 10. Pressure oscillations in function of α

Due to the behavior of the graph of α < 0, it is known as a converging or decaying behavior. Analogously, for α > 0 it is known as a diverging behavior. Also, as stated before, for α = 0 it is known as a neutral or critical behavior.

Recent contributions

Some recent contributions are presented here. By recent, it is being considered in the last 30 years, since it is when faster computers were introduced. Simpler

ISSN 1727-7337 (print)
ISSN 2663-2217 (online)

models were developed in order to obtain the droplet lifetime. Under a steady-state condition, applying energy and mass conservation and assuming Lewis number equal to 1, the mass rate of fuel vaporization is given by [5]:

$$\dot{m}_d = \frac{4\pi r_d k_g}{c_{p,g}} \ln(1+B). \quad (57)$$

It is valid to remember that, in this case, $B=B_T=B_M$. Now, the change in droplet diameter is calculated by the D² law, which is defined by:

$$\frac{dD_{d^2}}{Dt} = -\frac{8k_g}{\rho_L c_{p,g}} \ln(1+B), \quad (58)$$

where D_d is the droplet diameter. Since the derivative above is constant, D^2 varies linearly with the following slope [4]:

$$\kappa = -\frac{8k_g}{\rho_L c_{p,g}} \ln(1+B), \quad (59)$$

Then, the droplet lifetime is easily obtained by:

$$t_s = \frac{4r_d^2}{\kappa}\frac{D_{d,0}^2}{\kappa}, \quad (60)$$

where $D_{d,0}$ is the initial droplet diameter. It is important to remember that to evaluate the properties, it must be calculated in function of $\overline{T}$ .Fig. 11 shows the D² law graphically.

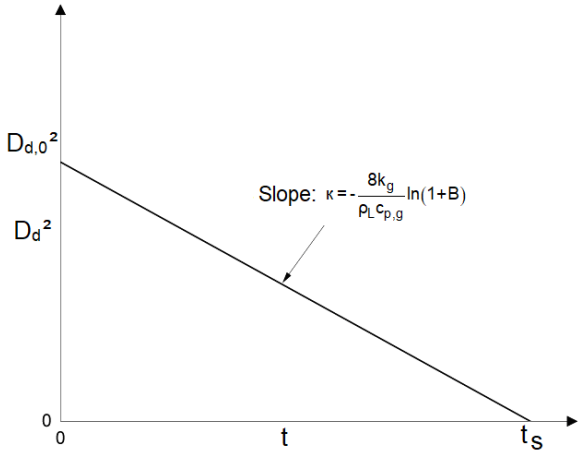

Fig. 11. D² law graphically

Although this model is quite useful, on applications that the droplet is in a high pressure and temperature atmosphere transient gets more relevant and must be modeled to consider the heat-up process [5]. Under transient condition there is $B_T \neq B_M$. In addition, remembering the heat transfer from the gas to the droplet is given in equation (8), the rate of change of surface temperature is calculated by:

$$\frac{dT_s}{dt} = \frac{q-q_v}{c_{p,L}m} = \frac{3\left[\dot{m}_d Q_b \left(\frac{B_T}{B_M}\right)-1\right]}{4c_{p,L}\rho_L r_d^3}, \quad (61)$$

where q_v is the heat used in vaporizing the fuel $(q_v = \dot{m}_d Q_b)$. An iterative method must be used to calculate the transient behavior and its stop point is when $B_T=B_M$, since when this equality is true, there is $q=q_v$ and the droplet finally heated up. Convective effects, such as the ones used ins Spalding's model, also can be used in this model. In addition, it is also possible to introduce the condition that the droplet is burning to the D² law [4]. Other constructive discussion about the D² law and droplets vaporization in quiescent atmospheres in general are presented in [41]. The D² law was developed decades ago, but some contributions are still taking place [43].

In [44,45] it was also considered, besides the other aspects already discussed, the turbulent intensity and velocity fluctuations influence on the droplet vaporization. The velocity fluctuation in function of the turbulent intensity is given below:

$$v_d = Iv_d = \frac{0.16v_d}{Re^{1/8}}, \quad (62)$$

where I is the turbulent intensity. In [3] the influence of turbulence is well discussed.

A two-dimensional transient model was developed by [46] to design gas turbines combustors. Although it is for gas turbines, it could be adapted for rocket engines. In this model, it was considered the fuel vaporization itself, but also droplets collisions, turbulent mixture and gases chemical kinetics, droplet heat-up and convective effects. Another model that considers similar aspects as the ones presented in [46] is the one from [47], but it considers a three-dimensional condition.

Recently, with the advancements of computational capacity, CFD (Computational Fluid Dynamics) models can consider many of the aspects already discussed in this work and others to be discussed in the next section. Especially with LES (Large Eddy Simulation) and DNS (Direct Numerical Simulation) models, but those numerical simulations are too costly, computationally. Those simulations could take from days to weeks to converge [10, 48-50]. A comparison of numerical simulations with the D² law was made by [51, 52] and it shows that the D² law is quite accurate.

All discussed models considered spherical droplets. However, the droplets deform due to the drag and thermal expansion (neglecting collisions). Some recent models consider these deformations, since it enhances the total and local mass and heat transfer and it demonstrated to be a relevant aspect to consider [51-57].

Other aspects, such as heat losses, usage of droplets distribution models, and many others are being studied until today [54, 55, 58].

Other factors to account

Some factors must be considered in some kinds of applications. The droplet behavior under near-critical, transcritical, and supercritical conditions should be accurately modeled for more precise results. In LPRE these conditions are commonly achieved, especially with LOX (Liquid Oxygen) droplets. These conditions are important to be modeled, mainly due to the fact that the surface tension coefficient of the vaporizing droplet tends to zero as the interface temperature reaches the critical conditions [25,59].

Other Aspect is the modeling of the vaporization of groups of droplets. This is a much more complex model, especially when adding multicomponent liquids, nonunitary Lewis number, combustion, and other factors. This type of model can also consider droplet-droplet collisions and droplet-wall collisions, and this is constantly occurring inside combustion chambers. Consequently, for a highly accurate model, these models are extremely important [3,25,59].

Considering real gas could also be an improvement to the algorithm. Ideal gas law is largely used in rocket engine internal ballistics theory, but it is a simplification [3].

Prediction of performance

As stated previously, in the case of too large chambers, heat losses may become larger and weight and costs increase. In the other hand, if the chamber is too small losses due to incomplete vaporization and combustion increases. In order to predict the C* efficiency due to incomplete vaporization, besides the equation (6), the following equation can be used [60]:

$$\eta_{C^*} = \frac{\left(C^*\right)_{O_{vap}/F_{vap}}}{\left(C^*\right)_{th}}\left(\frac{O_{vap}\dot{m}_o + F_{vap}\dot{m}_f}{\dot{m}_o + \dot{m}_f}\right), \quad (63)$$

where $\left(C^*\right)_{O_{vap}/F_{vap}}$ is the characteristic velocity in function of percentage of vaporized oxidizer or fuel, $\left(C^*\right)_{th}$ is the theoretical characteristic velocity for complete vaporization, O_{vap} is the percentage of vaporized oxidizer, F_{vap} is the percentage of vaporized oxidizer and, $\dot{m}_o$ and $\dot{m}_f$ are the theoretical oxidizer and fuel mass flow rate. It is valid to remember that $C^* = \frac{P_c A_t}{\dot{m}_o + \dot{m}_f}$. The Fig. 12 shows an example of η_{C^*} for ethanol/LOX in different mixture ratios $\left(O/F = \dot{m}_o/\dot{m}_f\right)$.

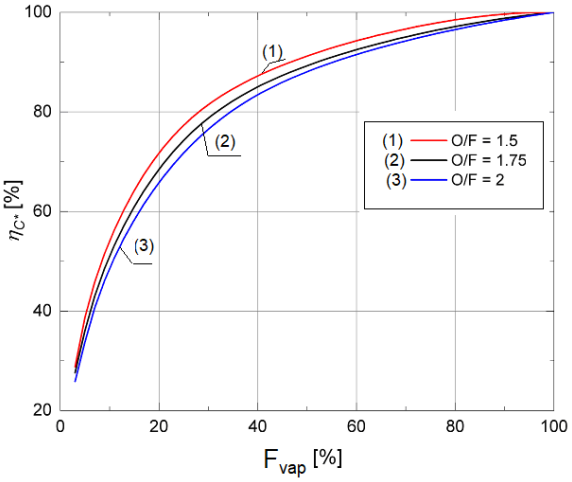

Fig. 12. η_{C^*} in function of percentage of vaporized fuel

Fig. 12 could also be made in function of percentage of vaporized oxidizer, however, in general, the oxidizer droplets vaporizes faster than fuel droplets [8], especially when it is being used cryogenic oxidizers and hydrocarbon fuels. In addition, [19] shows another form of equation (6) that could be used to calculate η_{C^*}.

As seen in Fig. 12, when the percentage of vaporized fuel reaches around 95% the efficiency gets to $\eta_{C^*} \rightarrow 100\%$. Then [10, 11] presents a correlation formula to calculate the required combustion chamber length in order to vaporize 95% of the propellant. This correlation was made for heptane, with an error band of ±10% therefore it is expected to predict with higher accuracy for similar fuels.

Conclusions

Various vaporization models were created, published and employed in Liquid Propellant Rocket Engines since the very beginning of the space race. Firstly, simpler models, such as one-dimensional ones, were presented. Through the years, with technological developments, the computational budget provided the possibility of more complex models to be developed, especially with numerical methods.

Combustion instabilities may be directly influenced by droplet vaporization, one of the theories that makes this correlation is the feed system coupled instabilities. The Summerfield criterion can be used in other to avoid this kind of instability, even though it is not a rule that always must be followed, as discussed. In addition, the vaporization impacts, also, directly on combus-

ISSN 1727-7337 (print)
ISSN 2663-2217 (online)

tion efficiency. Therefore, dominating this theory is of great importance on designing a LPRE.

References

1. Huzel, D. K., Huang, D. H. *Modern Engineering for Design of Liquid-Propellant Rocket Engines.* American Institute of Aeronautics and Astronautics Publ., 1992. 425 p.

2. Humble, R. W., Henry, G. N., Larson, W. J. *Space Propulsion Analysis and Design.* McGraw-Hill, Sep 1, 1995. 748 p.

3. Wang, Z. G. *Internal Combustion Processes of Liquid Rocket Engines: Modeling and Numerical Simulations.* National Defense Industry Press, Wiley Publ., 2016. 391 p.

4. Turns, S. R. *An Introduction to Combustion Concepts.* McGraw-Hill Publ., 3rd Ed., 2012. 752 p.

5. Lefebvre, A. H., McDonell, V. G. *Atomization and Sprays.* Taylor & Francis Group, LLC, 2017. 300 p.

6. Ghafourian, A. S., Mahalingam, S., Dindi, H., Daily, J. W. A Review of Atomization in Liquid Rocket Engines. 29th Aerospace Sciences Meeting, *AIAA 91-0283*, 1991. 10 p. DOI: 10.2514/6.1991-283.

7. Priem, R. J. *Propellant Vaporization as a Criterion for Rocket Engine Design; Calculations of Chamber Length to Vaporize a Single n-Heptane Drop*. NACA – National Advisory Committee for Aeronautics, Technical Note 3985, 1957. 41 p.

8. Spalding, D. B. A *One-Dimensional Theory of Liquid-Fuel Rocket Combustion.* Ministry of Supply Aeronautical Research Council, Imperial College of Science and Technology, London, 1959. 32p.

9. Gontijo, M. S., Fischer, G. A. A., Costa, F. S. Evaluation of SMD Effects on Characteristic Lengths of Liquid Rocket Engines Using Ethanol/LOx and RP-1/Lox. *18th Brazilian Congress of Thermal Sciences and Engineering*, 2020, pp. 1-10. DOI: 10.26678/ABCM.ENCIT2020.CIT20-0794.

10. Belal, H. M. *Numerical Simulation of Spray Combustion*. Master dissertation on Military Technical College (MTC), 2010. 300 p.

11. Belal, H. M. Validation of a Simplified Model for Liquid Propellant Rocket Engine Combustion Chamber Design. *IOP Conference Series Materials Science and Engineering*, 2020, pp. 1-15. DOI: 10.1088/1757-899X/973/1/012003.

12. Belal, H. M. Vaporization-Controlled Simplified Model for Liquid Propellant Rocket Engine Combustion Chamber Design. *IOP Conference Series Materials Science and Engineering*, 2019, pp. 1-15. DOI: 10.1088/1757-899X/610/1/012088.

13. Kessaev, J. V. *Theory and Calculation of Liquid-Propellant Engines*. Moscow Aviation Institute, Feb-Apr, 1997. 306 p.

14. Anderson, J. D. Jr. *Fundamentals of Aerodynamics.* McGraw Hill Education, 6th Ed., 2017. 1152p.

15. Anderson, J. D. Jr. *Modern Compressible Flow: With Historical Perspective*. McGraw Hill Education, 3rd Ed., 2002. 784 p.

16. Zucrow, M. J. Hoffman, J. D. *Gas Dynamics. Vol. 1.* John Wiley & Sons, Inc., 1976. 772 p.

17. Hill, P., Peterson, C. *Mechanics and Thermodynamics of Propulsion*. Addison Wesley Longman, 2nd Ed. Sep 1, 1992. 753 p.

18. Hugh, B. Mc. Numerical Analysis of Existing Liquid Rocket Engines as a Design Process Starter. *31st, AIAA/ASME/SAE/ASEE Joint Propulsion Conference*, July, San Diego, CA, 1995. 14 p. DOI: 10.2514/6.1995-2970.

19. Altman, D. Carter, J. M., Penner, S. S., Summerfield, M. *Liquid Propellant Rockets*. Princeton Legacy Library, 1960. 189 p.

20. Summerfield, M. A Theory of Unstable Combustion in Liquid Propellant Rocket Systems. *Journal of the American Rocket Society*, 1951, vol. 21, no. 5. 6 p. DOI: 10.2514/8.4374.

21. Priem, R. J. *Propellant Vaporization as a Criterion for Rocket Engine Design; Calculations Using Various Log-Probability Distributions of Heptane Drops*. NACA – National Advisory Committee for Aeronautics, Technical Note 4098, 1957. 29 p.

22. Clark, B. J., Hershc, M., Priem, R. J. *Propellant Vaporization as a Criterion for Rocket Engine Design; Calculations of Chamber Length to Vaporize Various Propellants*. NACA – National Advisory Committee for Aeronautics, Technical Note 3883, 1958. 37 p.

23. Priem, R. J. Vaporization of Propellants in Rocket Engines. *ARS Journal*, 1959, vol. 29. 6 p. DOI: 10.2514/8.4919.

24. Priem, R. J., Heidmann, M. F., *Propellant Vaporization as a Design Criterion for Rocket-Engine Combustion Chambers*. NASA Technical Report R-67, 1960, pp. 1-37.

25. Sirignano, W. A. *Fluid Dynamics and Transport of Droplets and Sprays*. 2nd Ed., Cambridge University Press, 2010. 480 p.

26. Ranz, W. E., Marshall, W. R. Evaporation from Drops. *Chemical Engineering Progress*, 1952, vol. 48, no. 3. 5 p.

27. Ingebo, R. D. *Vaporization Rates and Drag Coefficients for Isooctane Sprays in Turbulent Air Streams*. NACA – National Advisory Committee for Aeronautics, Technical Note 3265, 1954. 40 p.

28. Abramzon, B., Sirignano, W. A. Droplet Vaporization for Spray Combustion Calculations. *International Journal of Heat Mass Transfer*, 1989, vol. 32, no. 9, pp. 1605-1618. DOI: 10.1016/0017-9310(89)90043-4.

29. Aggarwal, S. K. A Review of Droplet Dynamics and Vaporization Modeling for Engineering Calculations. *Journal of Engineering for Gas Turbines and Power*, 1995, vol. 17, pp. 453-461. DOI: 10.1115/1.2814117.

30. Dipprey, D. F. Liquid Rocket Engines. *Chemistry in Space Research*. Elsevier, 1972, pp. 464-597,

31. Spalding, D. B. Combustion in Liquid-Fuel Rocket Motors. *Ministry of Supply Aeronautical Research Council*, Imperial College of Science and Technology, London, 1958. 27 p. DOI: 10.1017/S0001925900001402.

32. Spalding, D. B. The Combustion of Liquid Fuels. *International Symposium on Combustion*, 1953. 17 p. DOI: 10.1016/S0082-0784(53)80110-4.

33. Merouane, H., Bounif, A. Theoretical and Numerical Analysis of Fuel Droplet Vaporisation at High Temperatures. *WSEAS Transactions on Heat and Mass Transfer*, 2010, pp. 189-196.

34. Deprédurand, V., Castanet, G., Lemoine, F. Heat and Mass Transfer in Evaporating Droplets in Interaction: Influence of the fuel. *International Journal of Heat and Mass Transfer*, 2017, Elsevier, pp. 3495-3502. DOI: 10.1016/j.ijheatmasstransfer.2010.04.010.

35. Gontijo, M. S. *Preliminary Design, Analysis and Optimization of a Liquid Propellant Rocket Engine for Sounding Rockets* (in Portuguese). Monography Aerospace Engineering, University of Brasília, 2022. 286 p.

36. Khan, T. W., Qamar, I. Optimum Characteristic Length of Gas Generator for Liquid Propellant Rocket Engine. *Acta Astronautica*, Elsevier, 2020, vol. 176, pp. 1-12. DOI: 10.1016/j.actaastro.2020.06.021.

37. Gontijo, M. S., Fischer, G. A. A., Costa, F. S. Characteristic Lengths of Liquid Propellant Rocket Engines and the Influence of Chemical Reactions. *International Congress of Mechanical Engineering*, 2021, pp. 1-10. DOI: 10.26678/ABCM.COBEM2021.COB2021-2105.

38. Gontijo, M. S., Fischer, G. A. A., Costa, F. S. Influence of SMD on Characteristic Lengths of Liquid Propellant Rocket Engines. *8th Brazilian Combustion Institute Summer School of Combustion*, 2021. 10p.

39. Adler, J. A One-Dimensional Theory of Liquid-Fuel Rocket Combustion; Part II: The Influence of Chemical Reaction. *Ministry of Supply Aeronautical Research Council*, Imperial College of Science and Technology, London, 1959, pp. 1-20.

40. Williams, F. A. *Combustion Theory*. Benjamin/Cummings, 2nd Ed., 1985. 708 p.

41. Glassman, I., Yetter, R. A., Glumac, N. G. *Combustion*. Elsevier, 5th Ed., 2014. 774 p.

42. Ernst, R. L. L. *Liquid Rocket Analysis (LiRA); Development of a Liquid Bi-Propellant Rocket Engine: Design, Analysis and Optimization.* Master of Science dissertation, Master of Science in Spaceflight at Delft University of Technology, 2021. 188 p.

43. Law, C. K., Law, H. K. A d^2-Law for Multicomponent Droplet Vaporization and Combustion. *AIAA Journal*, 1982, vol. 20, no. 4, pp. 522-527. DOI: 10.2514/3.51103.

44. Khan, T., Qamar, I., Shah, F., Akhtar, K., Akhtar, R. Model for Fuel Droplet Evaporation in Combustion Chamber of Liquid Propellant Rocket Engines. *Journal of Engineering and Applied Sciences*, 2018, vol. 31, no. 1, pp. 1-10..

45. Khan, T., Qamar, I. Factors Affecting Characteristic Length of the Combustion Chamber of Liquid Propellant Rocket Engines. *Mehran University Research Journal of Engineering & Technology*, 2019, vol. 38, no. 3, pp. 729-744. DOI: 10.22581/muet1982.1903.16.

46. Raju, M. S., Sirignano, W. A. Multicomponent Spray Computations in a Modified Centerbody Combustor. *Journal of Propulsion and Power*, 1990, vol. 6, no. 2, pp. 97-105. DOI: 10.2514/3.23229.

47. Rizk, N. K., Mongia, H. C. Gas Turbine Combustor Design Methodology. *AIAA/ASME/SAE/ASEE Joint Propulsion Confference*, New York, 1986, pp. 1-11. DOI: 10.2514/6.1986-1531.

48. Wang, B., Kronenburg, A., Tufano, G. L., Stein, O. T. Fully Resolved DNS of Droplet Array Combustion in Turbulent Convective Flows and Modelling for Mixing Fields in Inter-Droplet Space. *Combustion and Flame*, 2018, vol. 189, pp. 347-366. DOI: 10.1016/j.combustflame.2017.11.003.

49. Farmer, R., Cheng, G., Chen, Y. CFD Simulation of Liquid Rocket Engine Injectors; Par 2. Simulations of the RCM-2 Experiment. *2nd International Workshop on Rocket Combustion Modeling: Atomization, Combustion and Heat Transfer*, 2001, pp. 1-12.

50. Duret, B., Qubeissi, M. A., Sazhin, S., Crua, C. Evaporating Droplets: Comparisons between DNS and Modelling. *ILAS, 26th Annual Conference on Liquid Atomization and Spray Systems*, Bremen-Germany, 2014, pp. 1-9. DOI: 10.13140/2.1.3258.8164.

51. Wang, Y., Yang, V. Vaporization of Liquid Droplet with Large Deformation and High Mass Transfer Rate, I: Constant-density, Constant-property case. *Journal of Computational Physics*, 2019, vol. 392, pp. 56-70. DOI: 10.1016/j.jcp.2019.03.013.

52. Wang, Y., Chen, X., Wang, X., Yang, V. Vaporization of Liquid Droplet with Large Deformation and High Mass Transfer Rate, II: Variable-density, Variable-property case. *Journal of Computational Physics*, 2019, vol. 394, pp. 1-17. DOI: 10.1016/j.jcp.2019.04.052.

53. Sahzin, S. S. Modelling of Droplet Heating and Evaporation. *University of Brighton*, 2017, pp. 45-75. DOI: 10.1007/978-981-10-7449-3_3.

54. Salvador, C. A. V. *Mathematical Model of Bipropellant Combustion Chambers* (in Portuguese). Masters Dissertation, INPE - National Space Research Institute, 2004. 215 p.

55. Salvador, C. A. V., Costa, F. S. Vaporization Lengths of Hydrazine Fuels Burning with NTO. *Journal of Propulsion and Power*, 2006, vol. 22, no. 6, pp. 1362-1372. DOI: 10.2514/1.18348.

56. Tonini, S., Cossali, G. E. One-dimensional Analytical Approach to Modelling Evaporation and Heating of Deformed Drops. *International Journal of Heat and Mass Transfer*, 2016, vol. 97, pp. 301-307. DOI: 10.1016/j.ijheatmasstransfer.2016.02.004.

57. Yang, S., Gao, Y., Cao, Y., Gu, Y., Gong, Z. Investigation on Deformation of an Evaporating Droplet in Convective Transcritical Enviroments. *Advances in Mechanical Engineering*, 2014, pp. 1-12. DOI: 10.1155/2014/326059.

58. Costa, E. M. S., Costa, F. S., Mendonça, M. T. 1.5D Model of Bipropellant Combustion Chambers (in Portuguese). *11° Workshop in Engineering and Space Technologies*, 2020. 9 p.

ISSN 1727-7337 (print)
ISSN 2663-2217 (online)

59. Sirignano, W. A. Fuel Droplet Vaporization and Spray Combustion Theory. *Progress in Energy and Combustion Science*, 1983, vol. 9, no. 4, pp. 291-322.

60. Heidmann, M. F., Priem, R. J. *Propellant Vaporization as a Design Criterion for Rocket-Engine Combustion Chambers; Relation Between Percentage of Propellant Vaporized and Engine Performance.* NACA – National Advisory Committee for Aeronautics, Technical Note 4219, 1958. 20 p.

Надійшла до редакції 25.04.2022, розглянута на редколегії 8.08.2022

ОГЛЯД МОДЕЛЕЙ ПАРОУТВОРЕННЯ ЯК КРИТЕРІЮ ПРОЕКТУВАННЯ ДВОПАЛИВНИХ ТЯГОВИХ КАМЕР

М. С. Гонтійо

На початку розробки рідкопаливних ракетних двигунів розміри тягової камери отримували, в основному, досвідченим шляхом. Завдяки технологічному прогресу протягом багатьох років було розроблено кілька підходів, щоб оптимізувати його розміри та точніше прогнозувати продуктивність. Окрім чіткого внеску в прогнозування ефективності, використання точних моделей пароутворення для оптимізації камер згоряння зменшує втрати та кількість необхідних випробувань. Щоб підвищити ефективність, камеру необхідно оптимізувати. Якщо камера занадто мала, досягається неповне згоряння і може виникнути нестабільність горіння. Якщо камера занадто велика, втрати від ваги та теплопередачі збільшуються, а транспортний засіб стає більше (що призводить до більших втрат на опору). Крім того, зменшується кількість тестів, оскільки моделі були експериментально перевірені, а для отримання оптимізованого дизайну потрібно менше експериментальних ітерацій. Хоча існує багато моделей, всі вони приходять до схожих висновків, наприклад, збільшення тиску в камері, зменшення розміру і швидкості введеної краплі та інші, призводять до зменшення необхідного розміру камери. Нині, з досягненням у обчисленні бюджету, можуть бути розроблені більш складні та точні моделі. Деякі з цих моделей враховують хімічні реакції, ефекти турбулентності, зіткнення та взаємодії крапель, дво- та тривимірне моделювання та інші. Крім того, використання кодів CFD дало відповідний внесок у аналітичні та числові моделі, особливо в їх валідацію, і, крім того, зменшує кількість необхідних експериментальних випробувань. Основним рушійним параметром, який керує цим явищем, є характерна довжина, яка враховує необхідний розмір камери для впорскування, розпилення, випаровування, змішування та спалювання палива. Більшість доступних моделей нехтують розпиленням, змішуванням і згорянням палива, оскільки ці явища відбуваються набагато швидше в порівнянні з пароутворенням. У цій роботі наведено огляд цих моделей випаровування, зосереджених на основних моделях, що використовуються у всьому світі. Цей вид огляду має велике значення для надання достатньої інформації та порівняння між моделями, що дає можливість досліднику/інженеру вибрати модель, яка краще відповідає її потребам, вимогам та обмеженням.

Ключові слова: моделі випаровування; рідкопаливні ракетні двигуни; характерна довжина; розмір введеної краплі.

Маурісіо Са Гонтіхо – Аерокосмічний інженер, Студент Магістратури Технологічний Інститут Аеронавтики, Аеронавігації та Машинобудування, Аерокосмічна Тяга та Енергетика, Бразилія.

Maurício Sá Gontijo – Aerospace Engineer, Master's Student at Technological Institute of Aeronautics, Aeronautical and Mechanical Engineering, Aerospace Propulsion and Energy, Brazil,
e-mail: mauricio.sa.gontijo@gmail.com, ORCID: 0000-0002-7648-0093.